

The Predicted Metallicity Distribution of Stars in Dwarf Spheroidal Galaxies

Gustavo A. Lanfranchi¹ and Francesca Matteucci²

¹*IAG-USP, R. do Matão 1226, Cidade Universitária, 05508-900 São Paulo, SP, Brazil*

²*Dipartimento di Astronomia-Università di Trieste, Via G. B. Tiepolo 11, 34131 Trieste, Italy*

15 September 2018

ABSTRACT

We predict the metallicity distribution of stars and the age-metallicity relation for 6 Dwarf Spheroidal (dSph) galaxies of the Local Group by means of a chemical evolution model which is able to reproduce several observed abundance ratios and the present day total mass and gas content of these galaxies. The model adopts up to date nucleosynthesis and takes into account the role played by supernovae of different types (II, Ia) allowing us to follow in detail the evolution of several chemical elements (H, D, He, C, N, O, Mg, Si, S, Ca, and Fe). Each galaxy model is specified by the prescriptions of the star formation rate and by the galactic wind efficiency chosen to reproduce the main features of these galaxies. These quantities are constrained by the star formation histories of the galaxies as inferred by the observed color-magnitude diagrams (CMD). The main conclusions are: i) five of the six dSphs galaxies are characterized by very low star formation efficiencies ($\nu = 0.005 - 0.5 \text{ Gyr}^{-1}$) with only Sagittarius having a higher one ($\nu = 1.0 - 5.0 \text{ Gyr}^{-1}$); ii) the wind rate is proportional to the star formation rate and the wind efficiency is high for all galaxies, in the range $w_i = 6 - 15$; iii) a high wind efficiency is required in order to reproduce the abundance ratios and the present day gas mass of the galaxies; iv) the predicted age-metallicity relation implies that the stars of the dSphs reach solar metallicities in a time-scale of the order of 2 - 6 Gyr, depending on the particular galaxy; v) the metallicity distributions of stars in dSphs exhibit a peak around $[\text{Fe}/\text{H}] \sim -1.8$ to -1.5 dex, with the exception of Sagittarius, which shows a peak around $[\text{Fe}/\text{H}] \sim -0.8$ dex; iv) the predicted metallicity distributions of stars suggest that the majority of stars in dSphs are formed in a range of metallicity in agreement with the one of the observed stars.

Key words: stars: metallicity distribution – galaxies: abundance ratios – galaxies: Local Group – galaxies: evolution –

1 INTRODUCTION

The metallicity distribution of stars and the age-metallicity relation (AMR) are very important constraints on chemical evolution models of all types of galaxies. The metallicity distribution of stars is representative of the chemical enrichment of the galaxy and provides information about the history of the chemical evolution and how it proceeded. The AMR, on the other side, provides information on the evolution with time of the Fe abundance in the interstellar medium (ISM) and in the stars. These two features, coupled with the abundance ratios of chemical elements, impose strong constraints on chemical evolution models and limit the range of acceptable values for several model parameters. In fact, the AMR and the metallicity distribution are affected by the choices of the initial mass function (IMF), the star formation rate (SFR) and the infall of gas (Tosi 1988),

whereas the abundance ratios depend mainly on the adopted nucleosynthesis, IMF and stellar lifetimes (Matteucci 1996).

In the Milky Way, the metallicity distribution of stars in the disc is, generally, estimated through G- and K- dwarf stars (see Kotoneva et al. 2002). These stars warrant a homogeneous sample and, since they have lifetimes equal to or greater than the age of the galaxy, they can provide a complete picture of the chemical enrichment of the Galaxy. The first observations compared to simple models of chemical evolution of our galaxy led to the so-called G- dwarf problem (van den Bergh 1962; Schmidt 1963), i.e. the number of metal-poor stars in the solar neighbourhood is lower than what is expected from predictions of the simple model (see Tinsley 1980; Matteucci 1996 for reviews). This problem has not been found either in the halo or in the bulge of the Galaxy (Carney et al. 1987; Laird et al. 1988; Macciò 1999). The first observations revealed a distribution in

the solar neighbourhood with almost no stars with $[\text{Fe}/\text{H}]$ lower than ~ -1.0 dex and two tentative peaks around ~ -0.4 dex and ~ 0.1 dex (Pagel 1989; Sommer-Larsen 1991). More recent observations using up-to-date techniques (Wyse & Gilmore 1995; Rocha-Pinto & Maciel 1996) and a more sophisticated chemical evolution model (Chiappini, Matteucci & Gratton 1997 - hereafter CMG97) solved the problem. The new distributions showed the same lack of very metal-poor stars but, contrary to the previous results, exhibited a well-defined peak in metallicity between $[\text{Fe}/\text{H}] = -0.3$ and 0 dex. This peak is well reproduced by the model of CMG97, which assumes a two-infall scenario for the formation of our Galaxy and correctly predicts a negligible number of stars with very low $[\text{Fe}/\text{H}]$, in agreement with the most recent G - and K- dwarf metallicity distributions.

In the bulge of the Milky Way, the metallicity distribution is estimated from oxygen abundance (given in the notation $(\text{O}/\text{H} = \log(\text{O}/\text{H}) + 12)$ observed in planetary nebulae (PN) (Ratag et al. 1997; Cuisinier et al. 1999). In such a case, there is a similarity with the metallicity distribution of the stars of the solar neighbourhood. There is a peak around $(\text{O}/\text{H}) = 8.7$, very few, if any, super metal rich objects with supersolar abundances and very few metal poor objects. In order to make a better comparison with the metallicity distribution of the disc stars, Maciel (1999) converted the O/H abundances into $[\text{Fe}/\text{H}]$ using the theoretical $[\text{O}/\text{H}]$ vs. $[\text{Fe}/\text{H}]$ relationship from Matteucci et al. (1999) for both the galactic bulge and solar neighbourhood. He concluded that the bulge distribution looks like the K giant distribution of the disc if the $[\text{O}/\text{H}]$ vs. $[\text{Fe}/\text{H}]$ relation for the solar neighbourhood is adopted. However, theoretical studies (Matteucci & Brocato 1990; Matteucci et al. 1999) have predicted a quite different $[\text{O}/\text{Fe}]$ vs. $[\text{Fe}/\text{H}]$ relation for the Bulge relative to the solar neighbourhood. In fact, they predicted that the majority of bulge stars should show $[\alpha/\text{Fe}] > 0$.

The age-metallicity relation is a poorer constraint on chemical evolution models for the Galaxy if compared to the metallicity distribution, since it can be reproduced very easily by various types of models. The extended data derived by Edvardsson et al. (1993) from F stars reveals a considerable scatter at almost all ages which can be reproduced easily by any model of chemical evolution. This scatter is, according to the authors, real and not due to observational uncertainties. In spite of that, the AMR exhibits a general behaviour of increasing metallicity with increasing galactic age, with a slope depending on the infall of gas, on the functional dependence of the SFR on the gas density and time, and on the adopted IMF (Tosi 1988; Sommer-Larsen & Yoshii 1990).

For Dwarf Spheroidal galaxies, unfortunately, neither the metallicity distribution of stars nor the AMR are available, making a comparison between model predictions and observations not yet possible. Very recently, however, a tentative metallicity distribution of stars was constructed for Sagittarius dSph (Bonifacio et al. 2004), but the number of data points is very low, allowing us to make only a qualitative comparison. In that sense, a true prediction that shall be confirmed or refuted by future observations can be obtained by means of chemical evolution models which are able to reproduce other observational constraints. We use in this paper the model from Lanfranchi & Matteucci (2003) (hereafter LM03) for dSphs in order to predict both the AMR and

metallicity distribution of stars in dSph galaxies. It is worth noting that the LM03 model is able to reproduce some observable features of dSphs, such as several abundance ratios, present day total mass and present day gas mass fraction, by treating in details the energetics and taking into account the yields of supernovae of type II (SNe II) and Ia (SNe Ia) as well as the yields of intermediate massive stars (IMS). The LM03 model explicitated the very important role of the galactic wind on the evolution of these galaxies and its effects on the abundance ratios, SFR, and final total and gas masses. The wind is characterized by its efficiency, i.e. the intensity of the rate of gas loss, which is assumed in LM03 to have the same efficiency for all galaxies. Possible differences in the rate of gas loss among these galaxies are accounted for by the different star formation (SF) efficiencies adopted for each galaxy, because the rate of the wind is assumed to be proportional to the SFR. In spite of that, we adopt in this work different wind efficiencies in order to get a better agreement with the observable data, namely the abundance ratios and HI mass/total mass fractions and to study the effect of different wind rates among galaxies. The other parameters of the model such as SFR, IMF, number, duration and epochs of the episodes of SF, remain the same as the ones in LM03. With this new approach, the AMR and the metallicity distribution of stars are predicted for a sample of 6 dSph galaxies of the Local Group and the influence of the galactic winds on these two features, as well as on the evolution of these galaxies, are analysed here.

The paper is organized as follows: in Sect. 2 we present the observational data concerning the dSph galaxies, in Sect. 3 the adopted chemical evolution models and star formation prescriptions are described, in Sect. 4 we describe the results of our models, and finally in Sect. 5 we draw some conclusions. We use the solar abundances measured by Grevesse & Sauval (1998) when the chemical abundances are normalized to the solar values ($[\text{X}/\text{H}] = \log(\text{X}/\text{H}) - \log(\text{X}/\text{H})_{\odot}$).

2 DATA SAMPLE

The data sample collected here is the same as in LM03, but now we restrict our study to only 6 galaxies of the Local Group which possess enough data to be compared to the predictions of the models. In that sense, we discard Fornax and Leo I and analyse the data from Draco, Sagittarius, Sculptor, Sextan, Ursa Minor and Carina. For these galaxies the data consists of abundances of iron and some α -elements such as O, Mg, Si and Ca obtained from the most recent high-resolution spectroscopy of red giant stars in these galaxies (Smecker-Hane & McWilliam 1999; Bonifacio et al. 2000; Shetrone, Coté & Sargent 2001; Shetrone et al. 2003; Bonifacio et al. 2004). Despite the relative small number of data points, it is possible to compare the observed abundance ratios with the model predictions. Besides the abundance ratios, we compare the results of the models to other properties of the dSph galaxies taken from the review of Mateo (1998) and use the star formation histories inferred from color-magnitude diagrams (Hernandez, Gilmore & Valls-Gabaud 2000; Dolphin 2002) as constraints on the number, epoch and duration of the episodes of SF. Unfortunately, there is no available data regarding both the AMR and the metallicity distribution of stars, with the exception

of Sagittarius, for which there is an observed metallicity distribution, but with a very low number of data points. The predictions are, therefore, compared only qualitatively to the abundances and ages of the observed stars.

3 MODELS

In this work we use the chemical evolution model for dSphs of LM03. The scenario representing the dSph galaxies is characterized by one or two long episodes of star formation (SF) and by the occurrence of very intense galactic winds. The model allows one to follow in detail the evolution of the abundances of several chemical elements, starting from the matter reprocessed by the stars and restored into the ISM by stellar winds and type II and Ia supernova explosions.

The main features of the model are:

- one zone with instantaneous and complete mixing of gas inside this zone;
- no instantaneous recycling approximation, i.e. the stellar lifetimes are taken into account;
- the evolution of several chemical elements (H, D, He, C, N, O, Mg, Si, S, Ca and Fe) is followed in detail;
- the nucleosynthesis prescriptions include the yields of: Thielemann, Nomoto & Hashimoto (1996) and Nomoto et al. (1997) for massive stars ($M > 10M_{\odot}$), van den Hoeck & Groenewegen (1997) for low and intermediate mass stars ($0.8 \leq M/M_{\odot} \leq 8$) and Nomoto et al. (1997) for type Ia supernovae. The type Ia SN progenitors are assumed to be white dwarfs in binary systems according the formalism originally developed by Greggio & Renzini (1983)

In our scenario, the dSph galaxies form through a continuous infall of pristine gas until a mass of $\sim 10^8 M_{\odot}$ is accumulated. One crucial feature in the evolution of these galaxies is the occurrence of galactic winds, which develop when the thermal energy of the gas equals its binding energy (Matteucci & Tornambé 1987). This quantity is strongly influenced by assumptions concerning the presence and distribution of dark matter (Matteucci 1992). A diffuse ($R_e/R_d=0.1$, where R_e is the effective radius of the galaxy and R_d is the radius of the dark matter core) but massive ($M_{dark}/M_{Lum} = 10$) dark halo has been assumed for each galaxy.

3.1 Theoretical prescriptions

The basic equation describing the evolution in time of the fractional mass of the element i in the gas within a galaxy, G_i , is:

$$\dot{G}_i = -\psi(t)X_i(t) + R_i(t) + (\dot{G}_i)_{inf} - (\dot{G}_i)_{out} \quad (1)$$

where $G_i(t) = M_g(t)X_i(t)/M_{tot}$ is the gas mass in the form of an element i normalized to a total fixed mass M_{tot} and $G(t) = M_g(t)/M_{tot}$ is the total fractional mass of gas present in the galaxy at the time t . The quantity $X_i(t) = G_i(t)/G(t)$ represents the abundance by mass of an element i , with the summation over all elements in the gas mixture being equal to unity. $\psi(t)$ is the fractional amount of gas turning into stars per unit time, namely the SFR. $R_i(t)$ represents the returned fraction of matter in the form of an element i that

the stars eject into the ISM through stellar winds and supernova explosions; this term contains all the prescriptions concerning the stellar yields and the supernova progenitor models. The infall of external gas and the galactic winds are accounted for by the two terms $(\dot{G}_i)_{inf}$ and $(\dot{G}_i)_{out}$, respectively. The prescription adopted for the star formation history is the main feature which characterizes the dSph galaxy models.

The SFR $\psi(t)$ has a simple form and is given by:

$$\psi(t) = \nu G(t) \quad (2)$$

where ν is the efficiency of star formation, namely the inverse of the typical time-scale for star formation, and is expressed in Gyr^{-1} .

In order to get the best agreement with the abundance ratios, total final mass, and final gas mass, ν is varied in each galaxy following the procedure and results of LM03. The star formation is not halted even after the onset of the galactic wind but proceeds at a lower rate since a large fraction of the gas ($\sim 10\%$) is carried out of the galaxy. The details of the star formation are given by the star formation history of each individual galaxy as inferred by CMDs taken from Dolphin (2002) and Hernandez, Gilmore & Valls-Gabaud (2000). It is adopted 1 or 2 episodes of SF, with durations that vary from 3 Gyr to 13 Gyr (see Table 1 for more details).

The rate of gas infall is defined as:

$$(\dot{G}_i)_{inf} = Ae^{-t/\tau} \quad (3)$$

with A being a suitable constant and τ the infall time-scale which is assumed to be 0.5 Gyr.

The rate of gas loss via galactic winds for each element i is assumed to be proportional to the star formation rate at the time t :

$$(\dot{G}_i)_{out} = w_i \psi(t) \quad (4)$$

where w_i is a free parameter describing the efficiency of the galactic wind. The wind is assumed to be differential, i.e. some elements, in particular the products of SNe Ia, are lost more efficiently than others from the galaxy (Recchi, Matteucci & D'Ercole 2001; Recchi et al. 2002). This fact translates into slightly different values for the w_i corresponding to different elements. Here we will always refer to the maximum value of w_i . The efficiency of the wind is different for each dSph galaxy.

The initial mass function (IMF) is usually assumed to be constant in space and time in all the models and is expressed by the formula:

$$\phi(m) = \phi_0 m^{-(1+x)} \quad (5)$$

where ϕ_0 is a normalization constant. Following LM03 we assume a Salpeter-like IMF (1955) ($x = 1.35$) in the mass range $0.1 - 100M_{\odot}$, but we also compare the predicted metallicity distributions to one from a model adopting a Scalo (1986) IMF.

In table 1 we summarize the adopted parameters for the models of dSph galaxies.

Table 1. Models for dSph galaxies. $M_{tot}^{initial}$ is the baryonic initial mass of the galaxy, ν is the star-formation efficiency, w_i is the wind efficiency, and n , t and d are the number, time of occurrence and duration of the SF episodes, respectively.

galaxy	$M_{tot}^{initial}(M_{\odot})$	$\nu(Gyr^{-1})$	w_i	n	$t(Gyr)$	$d(Gyr)$	IMF
Sextan	$5 * 10^8$	0.01-0.3	9-13	1	0	8	Salpeter
Sculptor	$5 * 10^8$	0.05-0.5	11-15	1	0	7	Salpeter
Sagittarius	$5 * 10^8$	1.0-5.0	9-13	1	0	13	Salpeter
Draco	$5 * 10^8$	0.005-0.1	6-10	1	6	4	Salpeter
Ursa Minor	$5 * 10^8$	0.05-0.5	8-12	1	0	3	Salpeter
Carina	$5 * 10^8$	0.02-0.4	7-11	2	6/10	3/3	Salpeter

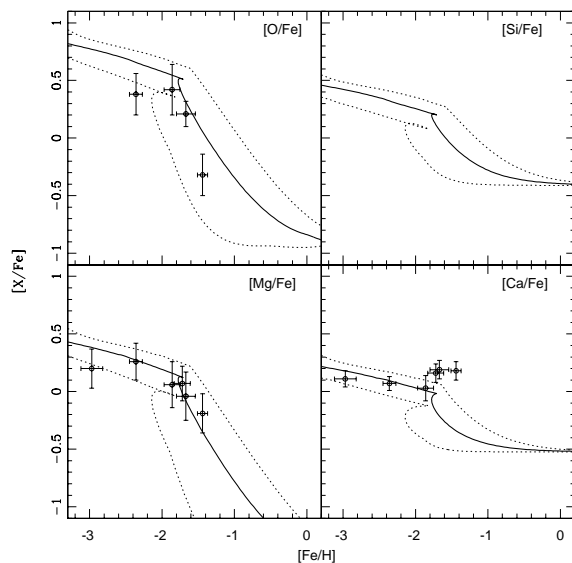
4 RESULTS

We compare the predictions from the chemical evolution models described in the previous section with some quantities, such as abundance ratios ($[O/Fe]$, $[Si/Fe]$, $[Mg/Fe]$, and $[Ca/Fe]$), total present day mass and total final gas mass, observed in a sample of 6 dSph galaxies from the Local Group. For each galaxy a model was built separately, using as a constraint for the SFR the SF histories inferred from CMDs (see Table 2). After defining the number, epoch and duration of the bursts (the other parameters are the same as in LM03), the SF efficiency and the wind efficiency were varied in order to best reproduce the observed abundance ratios and final total and gas masses (the model for each galaxy which gave the best agreement with the observed data was defined as the best model for that galaxy). The metallicity distribution of stars and the AMR were then computed by means of the best model for each of the 6 galaxies. We adopted, as first choices for the SF and wind efficiencies the values given in LM03: a SF efficiency in the range $\nu = 0.005 - 3 Gyr^{-1}$ and a wind efficiency of 10. The difference is that, in LM03 the wind efficiency was varied only for the standard model and kept the same in the models for individual galaxies, whereas here it is varied together with the SF efficiency in all models.

4.1 The $[\alpha/Fe]$ ratio

Abundance ratios are powerful tools in the study of chemical evolution of galaxies because they depend mainly on the nucleosynthesis prescriptions, stellar lifetimes and adopted IMF and not on the other model parameters. Some abundance ratios, such as the $[\alpha/Fe]$, can be used as "chemical clocks", providing information about the SF time-scale due to the difference in the formation and injection of these elements into the ISM. The α -elements are produced mainly in SNe II explosions in a short time-scale while the Fe-peak elements are produced in a much longer time-scale mainly in explosions of SNe Ia. Consequently, a low $[\alpha/Fe]$ implies a long SF time-scale and an older age whereas a high $[\alpha/Fe]$ ratio is the result of a short SF time-scale and a younger age.

The pattern of the $[\alpha/Fe]$ observed in Local Group dSph galaxies, showing generally lower $[\alpha/Fe]$ ratios at the same $[Fe/H]$ than in the Milky Way, is often considered difficult to explain (Tolstoy et al. 2003). This simply suggests that these galaxies are characterized by a low SFR. LM03 found that 6 galaxies of the Local Group have $[\alpha/Fe]$ ratios which can be well reproduced by a model characterized by low SF efficiencies in the range $\nu = 0.005 - 3 Gyr^{-1}$, depending on

**Figure 1.** $[\alpha/Fe]$ vs. $[Fe/H]$ observed in Draco dSph galaxy compared to the predictions of the chemical evolution model for Draco. The thick solid line represent the best model ($\nu = 0.03 Gyr^{-1}$, $w_i = 6$) and the dotted lines the lower ($\nu = 0.005 Gyr^{-1}$) and upper ($\nu = 0.1 Gyr^{-1}$) limits for the SF efficiency.

the galaxy, and by the consideration of intense differential galactic winds occurring in these galaxies.

We recover, in this work, the above analysis with a novelty relative to LM03. We vary also the wind efficiency in each galaxy in order to further explore the effects of the wind on the predicted abundance ratios and on the SF efficiencies, restricting, therefore, the range of acceptable values for this parameter. In Figures 1 to 6, the $[\alpha/Fe]$ ratios as functions of $[Fe/H]$ are shown in comparison with the predictions of the chemical evolution models for each of the 6 dSph galaxies (Draco, Sagittarius, Sculptor, Sextan, Ursa Minor and Carina, respectively). The solid lines correspond to the best model for each galaxy while the dashed lines represent the lower and upper limits for the SF efficiencies. As one can see, the models reproduce fairly well all the abundance ratios in every galaxy, in the ranges of SF and wind efficiencies given by the models. Some galaxies do not have all abundance ratios available and, in that case, only the predictions are shown. The range of SF efficiencies is almost the same for four galaxies: Carina ($\nu = 0.02 - 0.4 Gyr^{-1}$), Sculptor

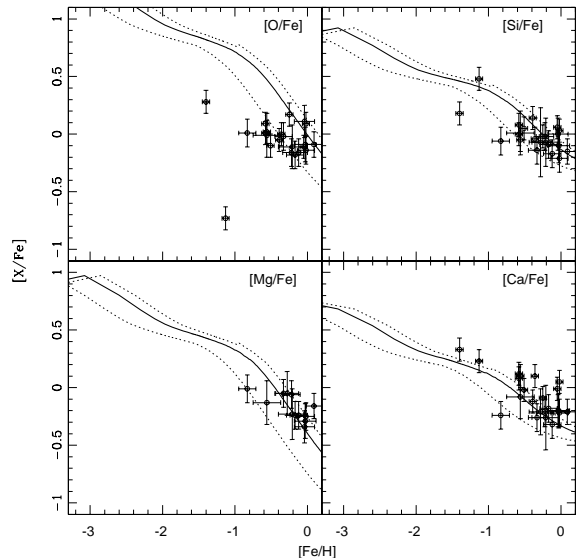


Figure 2. $[\alpha/\text{Fe}]$ vs. $[\text{Fe}/\text{H}]$ observed in Sagittarius *dSph* galaxy compared to the predictions of the chemical evolution model for Sagittarius. The thick solid line represent the best model ($\nu = 3 \text{ Gyr}^{-1}$, $w_i = 9$) and the dotted lines the lower ($\nu = 1 \text{ Gyr}^{-1}$) and upper ($\nu = 5 \text{ Gyr}^{-1}$) limits for the SF efficiency.

($\nu = 0.05 - 0.5 \text{ Gyr}^{-1}$), Ursa Minor ($\nu = 0.05 - 0.5 \text{ Gyr}^{-1}$) and Sextan ($\nu = 0.01 - 0.3 \text{ Gyr}^{-1}$). The other two galaxies are reproduced by higher values of the SF efficiency - Sagittarius ($\nu = 1.0 - 5.0 \text{ Gyr}^{-1}$) - and lower ones - Draco ($\nu = 0.005 - 0.1 \text{ Gyr}^{-1}$). The behaviour of the predicted abundance ratios is, though, very similar in all cases and consistent with the trend of the observed data: there is a sort of plateau in the abundance ratios for low metallicities ($[\text{Fe}/\text{H}] \leq \sim -1.8$, depending on the SF efficiency) followed by a sharp decrease which is more pronounced in the case of $[\text{O}/\text{Fe}]$ and $[\text{Mg}/\text{Fe}]$ than for $[\text{Si}/\text{Fe}]$ and $[\text{Ca}/\text{Fe}]$.

This sudden decrease in the predicted abundance ratios is a consequence of the occurrence of galactic winds and of the injection of Fe in the ISM of the galaxy by SNe Ia. As soon as the wind starts the SF declines fast due to the decrease in the amount of the available gas almost halting the formation of new stars and, consequently, the production and injection of α elements into the ISM by SNe II. The Fe-peak elements, on the other hand, are continuously injected into the ISM by SNe Ia, since these explosions start occurring several Myr ($> 30 \text{ Myr}$) after the onset of the SF and continue, even if the SF is halted, for several Gyrs (up to 10) due to the long lifetimes of the stars responsible for this type of explosion. These two facts are the main responsible for the general decrease of the $[\alpha/\text{Fe}]$ ratios after the onset of the wind. The differences between the pattern of the $[\text{Ca}$, $\text{Si}/\text{Fe}]$ and that of $[\text{O}$, $\text{Mg}/\text{Fe}]$ ratios reflect this behaviour. There is a smoother decrease in $[\text{Ca}/\text{Fe}]$ and $[\text{Si}/\text{Fe}]$, since Ca and Si are produced also in SNe Ia and an abrupt one in $[\text{O}/\text{Fe}]$ and $[\text{Mg}/\text{Fe}]$, because the production of O and Mg in SNe Ia is negligible.

The effects of the differential aspect of the wind are clearly seen, though, only in the models with the lowest SF efficiencies and in the absolute Fe abundance (see LM03).

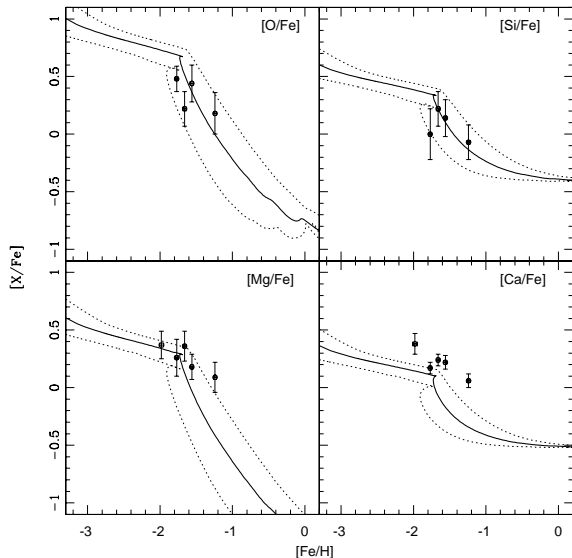


Figure 3. $[\alpha/\text{Fe}]$ vs. $[\text{Fe}/\text{H}]$ observed in Sculptor *dSph* galaxy compared to the predictions of the chemical evolution model for Sculptor. The thick solid line represent the best model ($\nu = 0.2 \text{ Gyr}^{-1}$, $w_i = 13$) and the dotted lines the lower ($\nu = 0.05 \text{ Gyr}^{-1}$) and upper ($\nu = 0.5 \text{ Gyr}^{-1}$) limits for the SF efficiency.

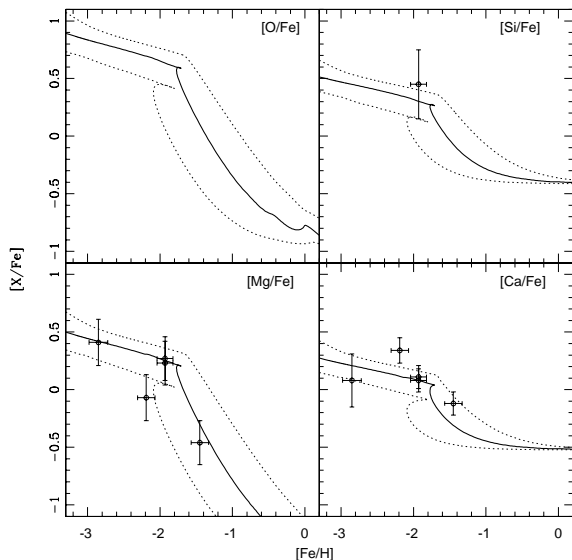


Figure 4. $[\alpha/\text{Fe}]$ vs. $[\text{Fe}/\text{H}]$ observed in Sextan *dSph* galaxy compared to the predictions of the chemical evolution model for Sextan. The thick solid line represent the best model ($\nu = 0.08 \text{ Gyr}^{-1}$, $w_i = 9$) and the dotted lines the lower ($\nu = 0.01 \text{ Gyr}^{-1}$) and upper ($\nu = 0.3 \text{ Gyr}^{-1}$) limits for the SF efficiency.

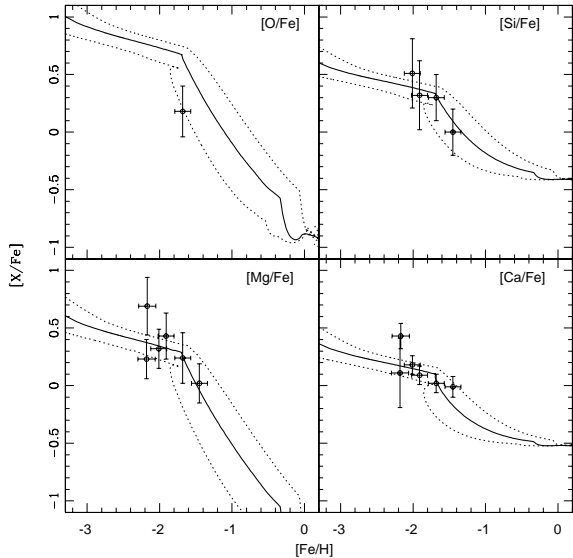


Figure 5. $[\alpha/\text{Fe}]$ vs. $[\text{Fe}/\text{H}]$ observed in Ursa Minor dSph galaxy compared to the predictions of the chemical evolution model for Ursa Minor. The thick solid line represent the best model ($\nu = 0.2 \text{ Gyr}^{-1}$, $w_i = 10$) and the dotted lines the lower ($\nu = 0.05 \text{ Gyr}^{-1}$) and upper ($\nu = 0.5 \text{ Gyr}^{-1}$) limits for the SF efficiency.

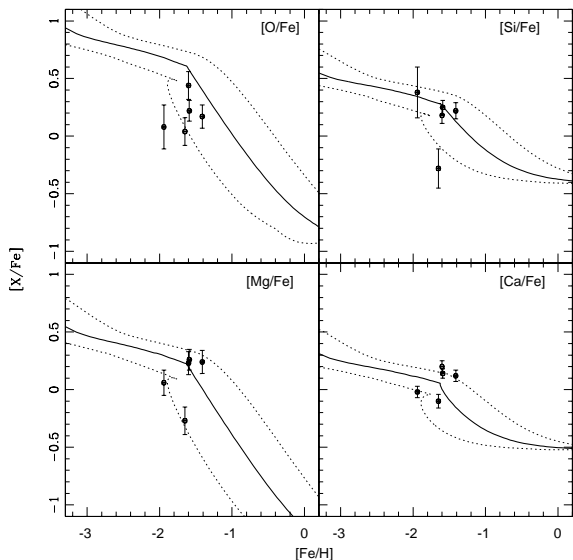


Figure 6. $[\alpha/\text{Fe}]$ vs. $[\text{Fe}/\text{H}]$ observed in Carina dSph galaxy compared to the predictions of the chemical evolution model for Carina. The thick solid line represent the best model ($\nu = 0.1 \text{ Gyr}^{-1}$, $w_i = 7$) and the dotted lines the lower ($\nu = 0.02 \text{ Gyr}^{-1}$) and upper ($\nu = 0.4 \text{ Gyr}^{-1}$) limits for the SF efficiency.

The intensity of the wind, on the other hand, is very important to reproduce the abundance ratios, especially the ones with the lowest values at higher metallicities. Generally, if the efficiency of the wind is increased, the decrease in the abundance ratios is more pronounced and the predicted values are lower after the onset of the wind. This is caused by the influence of the wind on the SF: the more intense is the wind, the lower is the SFR after the onset of the wind, since a higher fraction of gas ($\sim 10\%$) is lost from the galaxy. In this sense, only an intense and differential wind can account for the lowest values observed in these galaxies. The intensity of the wind is characterized by the wind efficiency, which lies in similar ranges for all the dSph galaxies studied here, close to the values defined for the models of LM03 (see Table 1). The best model for each galaxy, on the other hand, adopts wind efficiencies which differ considerably. While the best model for Draco and Carina requires the lowest wind efficiencies ($w_i = 6$ and 7 , respectively) and for Sculptor the highest one ($w_i = 13$), the wind efficiency of the best models for Ursa Minor, Sextan and Sagittarius assume intermediate values ($w_i = 10$, 9 and 9 , respectively). The differences in the best value and the similarity in the range of acceptable values of the wind efficiency for all galaxies reflects the fact that each galaxy follows a particular track of evolution, but they all resemble to each other, as already noticed for the SF efficiency.

The total final mass and final gas mass observed are also compared to the predictions of the models (see Table 2). The ranges in the predicted values of the total mass and HI/total mass ratio for each galaxy are a consequence of the variations in the SF and wind efficiencies. As the efficiency of the wind is increased the total mass and final gas mass decrease, since more gas is lost from the galaxy. Besides that, the total mass of stars is also lower since the decrease in the SFR after the onset of the wind is more pronounced for higher values of the wind efficiency. The SF efficiency, on the other hand, acts in an opposite way. If it is increased, the final total mass and present day gas mass are also increased. These effects, however, are less important than the ones due to the different wind efficiencies. Consequently, the range of values adopted for the wind efficiency for each galaxy produces a range of predicted masses for each model galaxy. In particular, the range of adopted values for the wind and SF efficiencies gives final gas masses in agreement with what is inferred from observations, suggesting that our assumptions on galactic winds and SFR are quite reasonable.

4.2 The age-metallicity distribution

In Figures 7 to 12, the predicted age-metallicity relation is plotted for Draco, Sagittarius, Sculptor, Sextan, Ursa Minor and Carina, respectively. The solid lines represent the best model for each galaxy and the dotted lines the upper and lower limits on the SF efficiency. In general, the metallicity, represented by the predicted $[\text{Fe}/\text{H}]$, increases with time reaching solar values between 2 to 6 Gyr after the onset of the SF. This time-scale depends on the details of the SF, such as the SF efficiency and the SF history of the galaxy. Concerning the SF history, the galaxies can be divided in to two distinct groups: one with galaxies in which the SF starts at the beginning of the formation (by gas assembly) of the galaxy by gas accretion and another one with the galaxies

Table 2. Predictions of the models for dSph galaxies compared to observations. M_{tot}^{final} is the present day total mass of the galaxy, M_{HI}/M_{tot} is the present day ratio between the HI mass and total mass.

	M_{tot}^{final} ($10^6 M_{\odot}$)		$M_{HI}/M_{tot} \cdot 10^{-3}$		1 ^o burst (Gyr)		2 ^o burst (Gyr)	
	obs	mod	obs	mod	obs	mod	obs	mod
Draco	22 ^a	5.53-25.5	<1 ^a	0.2-0.8	6-10 ^b	6-10	-	-
Sagittarius	-	70.4-214	<1 ^a	0.2-0.3	0-13 ^c	0-13	-	-
Sextan	19 ^a	6.19-28.9	<1 ^a	0.1-0.4	-	0-8	-	-
Sculptor	6.4 ^a	10.2-31.2	4 ^a	0.1-0.4	0-7 ^c	0-7	-	-
Ursa Minor	23 ^a	11.3-38	<2 ^a	0.2-0.4	0-3 ^b	0-3	-	-
Carina	13 ^a	9.72-58	<1 ^a	0.2-0.6	6-9 ^b	6-9	10-13 ^b	10-13

a - Mateo (1998)

b - Hernandez, Gilmore & Valls-Gabaud (2000)

c - Dolphin (2002)

d - for the whole sample of dSph galaxies in Mateo (1998)

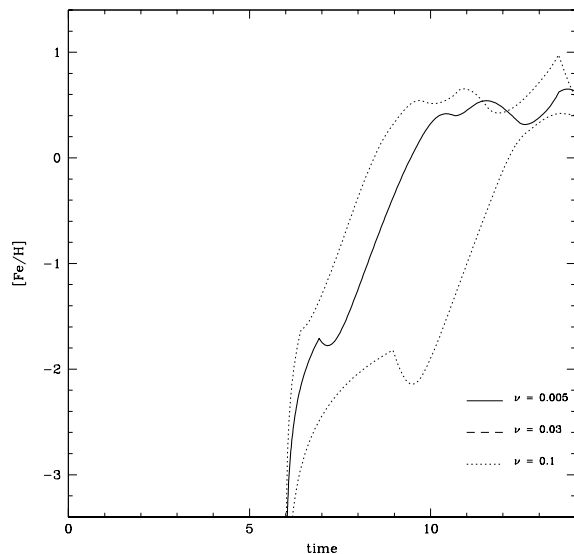


Figure 7. $[Fe/H]$ as a function of time as predicted by the model for Draco. The solid line represents the best model and the dotted lines the upper and lower limits on the SF efficiencies.

in which the SF starts several Gyr after the formation of the galaxy. Carina and Draco are part of the second group and the remaining galaxies, Sagittarius, Sextan, Sculptor and Ursa Minor, form the group of galaxies with SF occurring since the beginning of formation of the system.

The difference in the epoch of the onset of the SF between the two groups reflects other major differences. In Draco and Carina the metallicity rises fast reaching solar values in a few Gyr, between 2.5 to 6 Gyr in Draco and 1.5 to 3.5 Gyr in Carina. In Carina the rise is faster due to the higher SF efficiency ($\nu = 0.02 - 0.4 \text{ Gyr}^{-1}$) compared to Draco ($\nu = 0.005 - 0.1 \text{ Gyr}^{-1}$). This behaviour implies that the ages of the observed stars of these galaxies should be low, since they started forming around 8 - 9 Gyr ago and reached solar chemical composition in the gas $\sim 2 - 3 \text{ Gyr}$ later, and that the spread in their ages should be relatively small, $\sim 2 - 3 \text{ Gyr}$ for the best model of each galaxy. The spread in the ages of the observed stars is inferred considering that all

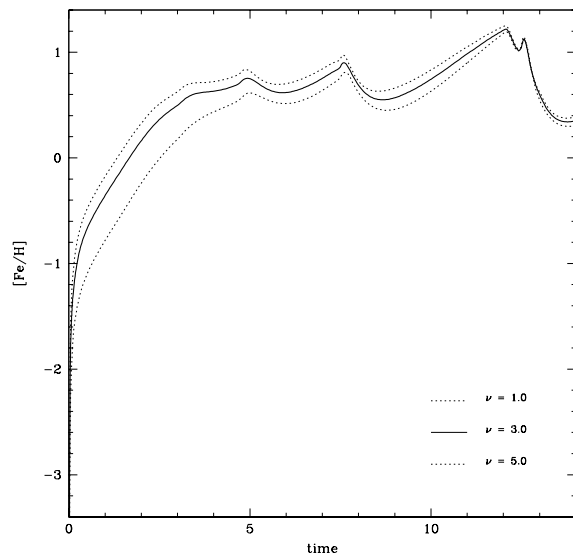


Figure 8. $[Fe/H]$ as a function of time as predicted by the model for Sagittarius. The solid line represents the best model and the dotted lines the upper and lower limits on the SF efficiencies.

the observed stars have $[Fe/H]$ lying in the range -3.0 to 0.0 dex and assuming the SF history inferred by the observed CMDs. However, both the spread in gas abundances and the time-scale necessary to reach the solar metallicities strongly depend on the adopted SF efficiency.

If one considers the models with the lower limit on the SF efficiency the spread in the ages among the stars will be between (~ 3.5 to $\sim 6 \text{ Gyr}$) and the metallicities will take longer to reach solar values. On the other hand, if ν is larger, these time intervals will be shorter, the spread in the ages of the stars narrower and the dominant stellar population will be older. Tolstoy et al. (2003) have derived age-metallicity relations for Carina and Sculptor. However, a meaningful comparison between our age-metallicity relations and theirs is not possible since we adopted SFHs different from the ones they adopt. In particular, there is a discrepancy between our stellar ages and those inferred by Tolstoy et al. (2003) for Carina. In our opinion, firm conclusions on this point cannot

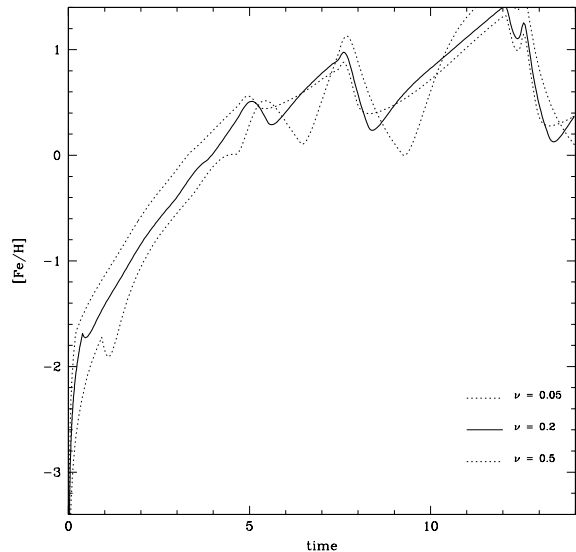


Figure 9. $[\text{Fe}/\text{H}]$ as a function of time as predicted by the model for Sculptor. The solid line represents the best model and the dotted lines the upper and lower limits on the SF efficiencies.

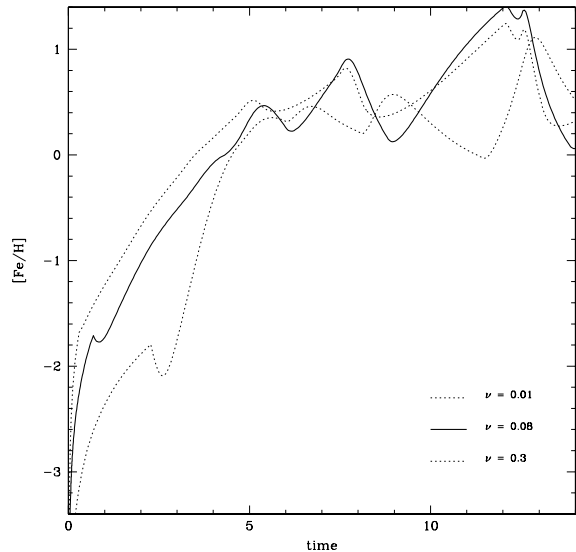


Figure 10. $[\text{Fe}/\text{H}]$ as a function of time as predicted by the model for Sextan. The solid line represents the best model and the dotted lines the upper and lower limits on the SF efficiencies.

still be drawn, because of the many uncertainties affecting the derivation of stellar ages. Anyway, what is interesting to note is that our assumed SFHs well reproduce the abundance patterns ($[\alpha/\text{Fe}]$ vs. $[\text{Fe}/\text{H}]$).

The other group of galaxies, the ones with a SF beginning as soon as the galaxy starts forming (Sculptor, Sextan, Ursa Minor and Sagittarius), exhibit a different behaviour. In this case, the dependence of the AMR on the SF efficiency is weak and the results for the best model apply also to the models with the lower and upper limits on the SF efficiency.

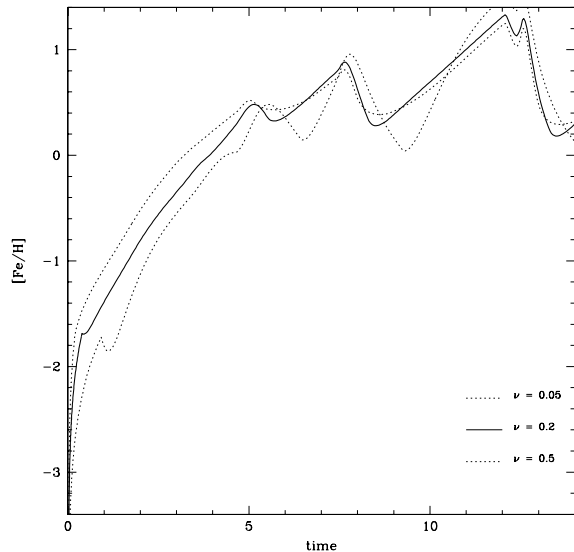


Figure 11. $[\text{Fe}/\text{H}]$ as a function of time as predicted by the model for Ursa Minor. The solid line represents the best model and the dotted lines the upper and lower limits on the SF efficiencies.

The rise of the $[\text{Fe}/\text{H}]$ with time is less steep and it is necessary ~ 4 Gyr for the ISM to reach solar metallicities. This implies a larger range for the stellar ages in these galaxies, between $\sim 3.5 - 4.5$ Gyr for Sextan and Ursa Minor and $\sim 3.5 - 4.75$ Gyr for Sculptor, in agreement with the ages derived observationally (Tolstoy et al. 2003). A fraction of the stars would be also older than ~ 10 Gyr since they started forming around 14 Gyr ago (assuming that the Universe has 15 Gyr) and would have reached solar metallicities 4 Gyr later. Sagittarius, however, does not follow this behaviour. Even though the SF in this galaxy starts as soon as the galaxy forms, the rise in the $[\text{Fe}/\text{H}]$ is very fast (~ 2 Gyr) due to the higher SF efficiency compared to the other dSph galaxies. Because of these two facts, the stars of Sagittarius would be the oldest ones (with ages ~ 12 Gyr) among the stars observed in dSph galaxies. The fact that the stars of Sagittarius should be old may lead to the idea that they should also be less enriched, but, as the SF is very efficient in this galaxy, the chemical enrichment of the ISM is very efficient too. In this way the stars of Sagittarius, although old, are also metal rich. In fact, it is meaningless to compare the metallicities of the stars of different galaxies according to their age, because each galaxy has had a particular evolution with a particular SF, even though there are similarities among the SF histories of the local dSph galaxies.

It is worth noting that all the model galaxies, independently of the adopted SF history or SF efficiency, exhibit, however, peaks in the AMR. As the adopted SF is characterized by long episodes (> 3 Gyr) of activity one should expect a continuous increase in metallicity, contrary to what is predicted by the models. Actually, even though the episodes of SF are long, the rate of SF is not constant over time and decreases substantially after the onset of the wind due to the removal of a large fraction of the gas reservoir which fuels the SF. The formation of new stars is, consequently, almost halted and the injection of Fe into the ISM is negligible, ex-

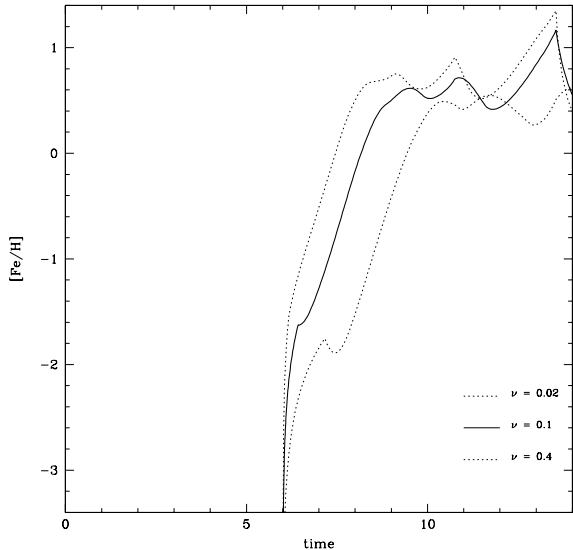


Figure 12. $[\text{Fe}/\text{H}]$ as a function of time as predicted by the model for Carina. The solid line represents the best model and the dotted lines the upper and lower limits on the SF efficiencies.

cept for the sporadic contribution of SNe Ia explosions. In this sense, the increase of the metallicity in the ISM is much less intense and, sometimes, there is even a decrease due to the preferential loss of Fe by means of differential galactic winds. The peaks seen in the predicted AMR are, then, a result of an interplay between the injection of Fe into the ISM by SNe Ia explosions (when the $[\text{Fe}/\text{H}]$ increases) and the preferential loss of Fe by galactic winds (causing the decrease). This behaviour is responsible also for maintaining an almost constant mean metallicity several Gyr after the beginning of the SF.

4.3 The stellar metallicity distribution

The predicted metallicity distribution of stars of the Milky Way (MW) disc at the solar neighbourhood compared to the ones predicted by the best model for Draco, Sagittarius, Sextan, Sculptor, Ursa Minor and Carina are shown in Figures 13 to 18, respectively. For Sagittarius the predicted metallicity distribution is compared also to the data of Smecker-Hane & Mc. William (1999) and Bonifacio et al. (2004). The solid lines represent the predictions for the best model selected for each *dSph* galaxy, the dotted line the predicted distribution of the model of CMG97 for the solar vicinity in the disc of the MW, which well reproduces the observed one, and the dashed line the observational distribution for Sagittarius.

In general, the *dSph* galaxies exhibit distributions qualitatively similar to the one predicted for the solar vicinity: there is a unique distinct peak in the relative number of stars formed at a given metallicity. This is, however, the only similarity between the distributions of the solar neighbourhood and the *dSph* galaxies. The position in metallicity of the peak, its width and the slope of the distribution function are different, not only between the *dSph* galaxies and our Galaxy, but also between the *dSph*s themselves.

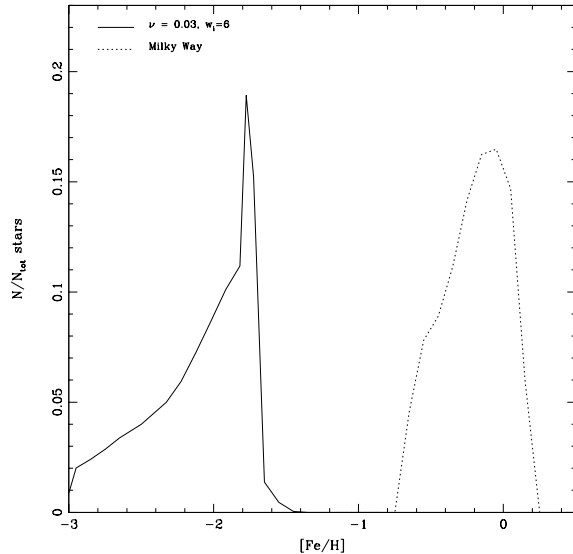


Figure 13. The distribution of stars as a function of $[\text{Fe}/\text{H}]$ predicted by the best model for Draco compared to the distribution of the Milky Way model (dotted line).

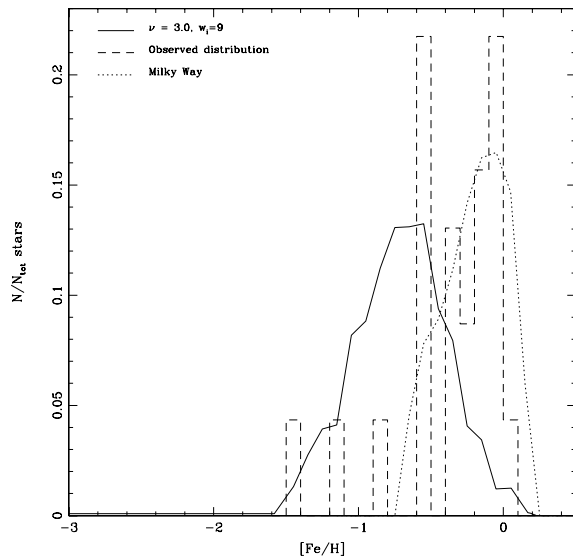


Figure 14. The distribution of stars as a function of $[\text{Fe}/\text{H}]$ predicted by the best model for Sagittarius compared to the distribution of the Milky Way model (dotted line) and to the observed one (dashed line)(see text).

In general, the peak of the metallicity distribution in the *dSph*s occurs at lower metallicities than the one in the solar neighbourhood. The position of the peak, though, is specific for each galaxy. While Sagittarius has a peak near the one of the Milky Way (at $[\text{Fe}/\text{H}] \sim -0.8$ dex in Sagittarius and at $[\text{Fe}/\text{H}] \sim -0.1$ dex in the MW), for Draco the peak is at $[\text{Fe}/\text{H}] \sim -1.8$ dex. Generally, in the *dSph*s the peak is situated around ~ -1.6 dex, almost 1.5 dex below the value of the solar vicinity, but close to the value inferred for the

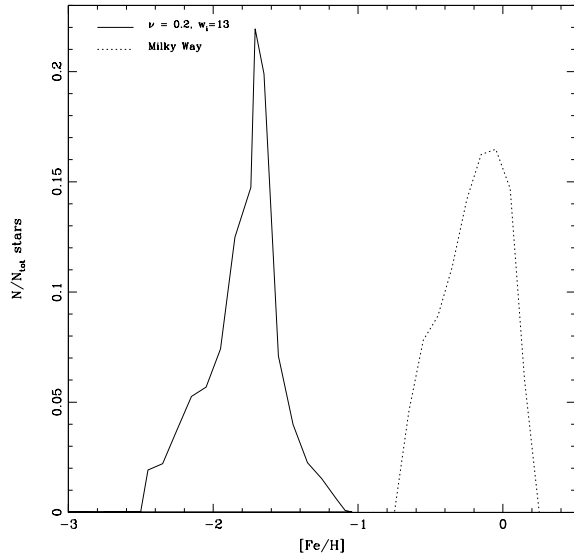


Figure 15. The distribution of stars as a function of $[Fe/H]$ predicted by the best model for Sculptor compared to the distribution of the Milky Way model (dotted line).

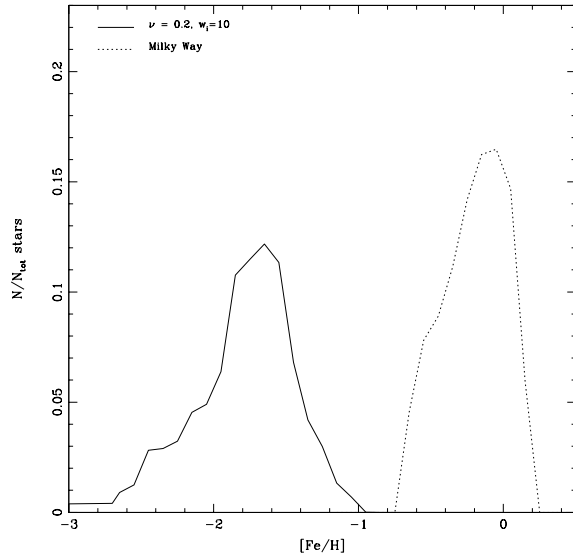


Figure 17. The distribution of stars as a function of $[Fe/H]$ predicted by the best model for Ursa Minor compared to the distribution of the Milky Way model (dotted line).

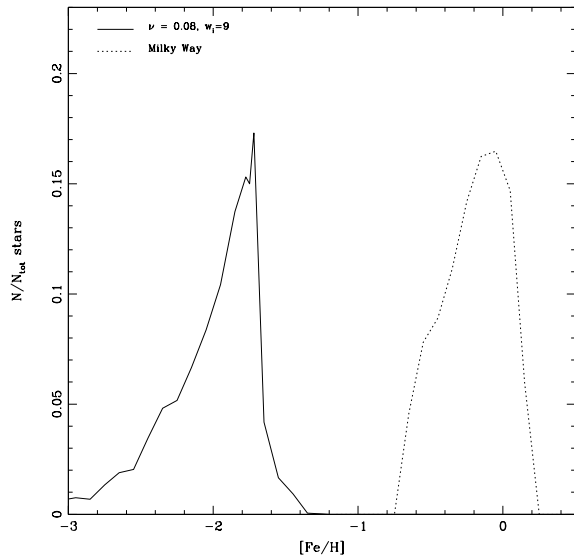


Figure 16. The distribution of stars as a function of $[Fe/H]$ predicted by the best model for Sextan compared to the distribution of the Milky Way model (dotted line).

halo metallicity distribution, which lies around $[Fe/H] \sim -1.55$ dex (Laird et al. 1988). The difference between the peak of the dSph metallicity distributions and the one of the solar vicinity is due to the fact that the dSph galaxies exhibit a lower SF efficiency than the MW disc, so the typical metallicity of the formed stars is lower than the one of the disc of our galaxy at the solar vicinity. Besides that, the occurrence of the intense galactic wind prevents the dSph galaxies to form stars with relatively high metallicities, since it carries away a large fraction of the gas of the galaxy, thus decreasing

the SF which almost stops shortly after the time at which the wind develops (at $[Fe/H] \sim -1.4 - -1.2$ dex). This fact is more clearly seen in the high metallicity end of the distributions. One can easily notice for Draco, Carina, Sculptor and Sextan a sudden and intense decrease in the metallicity distribution after the peak. This is the effect of the intense wind on the number of stars formed: the SF does not cease completely, but decreases substantially, thus decreasing also the number of stars formed at metallicities larger than the ISM metallicity at the time of the wind. The exact value of this metallicity depends strongly on the SF efficiency but weakly on the wind efficiency. On the other hand, the efficiency of the wind is very important in predicting the decrease of the distribution after the peak: the higher is the wind efficiency, the more intense is the decrease and the lower is the number of stars formed after that.

The extension toward low metallicities of the predicted metallicity distribution in dSph galaxies exhibits a different pattern than the one of our Galaxy. In the solar neighbourhood, there are almost no stars formed with metallicities lower than ~ -1.0 dex (the so called G-dwarf problem) contrary to the dSph galaxies where there are stars with metallicities well below the one of the peak. This is due to the long infall time-scale required by the metallicity distribution in the solar vicinity ($\sim 7 - 8$ Gyrs) as opposed to the short infall time-scale assumed for dSphs (0-5 Gyrs). The spread in the metallicity of the majority of stars in dSph galaxies is, consequently, larger than in the solar neighbourhood. While in the MW the metallicity distribution of stars spans ~ 1.0 dex in metallicity, in the dSph it reaches ~ 1.6 dex. This difference is related to the much lower SF rate in the dSph galaxies when compared to the one of the disc of the MW ($\nu = 1 \text{Gyr}^{-1}$, see CMG97).

Even though there is no available data to make a comparison with the predicted distributions in dSph galaxies (with the exception of Sagittarius) it should be noticed that

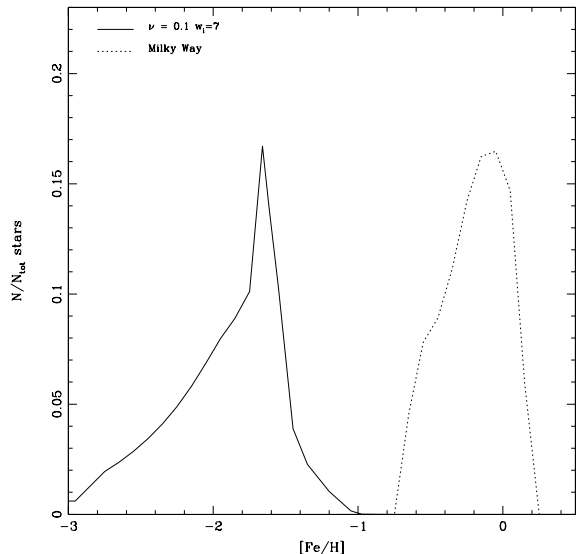


Figure 18. The distribution of stars as a function of $[\text{Fe}/\text{H}]$ predicted by the best model for Carina compared to the distribution of the Milky Way model (dotted line).

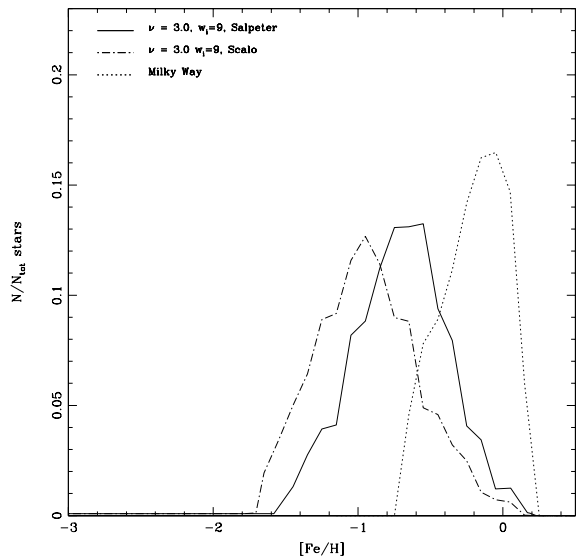


Figure 19. The distribution of stars as a function of $[\text{Fe}/\text{H}]$ predicted by the model for Sagittarius with a Scalo IMF (dotted dashed line) and a Salpeter IMF (solid line) compared to the distribution of the Milky Way model (dotted line).

the peaks for all galaxies lie in the same range of metallicities of the observed stars in each galaxy. This suggests that the proposed models are reasonable. In the case of Sagittarius, as the number of the data points is very low, the comparison with the predictions is only qualitative. In that sense, the best model reproduces very well the observed distribution, since the predicted range of metallicities of the formed stars is the same of the observed ones. The position of the peak of the observed distribution is not statistically meaningful

and should be confirmed or refuted by a more complete data sample.

Finally, we computed a model similar to the one for Sagittarius but with a Scalo IMF in order to test the effect of a different IMF and to compare more precisely the predicted metallicity distribution of dSph galaxies with the one of the model of CMG97 for the MW disc, which adopts a Scalo IMF. When this IMF is adopted for the dSph galaxies the predicted metallicity distribution is pushed toward lower values of metallicities and the peak of the distribution occurs at lower $[\text{Fe}/\text{H}]$ values. Consequently, only the observed stars with the lowest metallicities are fitted by the distributions predicted by the model with Scalo IMF, that is unable to reproduce the stars with the highest metallicities. This fact together with the fact that a model with Scalo IMF is unable also to reproduce the abundance ratios (LM03) makes clear that this choice of IMF is not suited for the dSph galaxies, which are better reproduced by a Salpeter one.

5 SUMMARY

We first analysed the star formation and chemical evolution in 6 dSph galaxies of the Local Group comparing several observed abundance ratios to the predictions of detailed chemical evolution models. After defining the best models for each galaxy, which are specified by the SF history inferred by observed CMDs and by the adopted SF and wind efficiencies, we predicted the metallicity distribution of stars and the age-metallicity relation for each dSph of the sample. By taking into account the role played by supernovae of different types (II, Ia) and adopting up to date nucleosynthesis prescriptions we followed the evolution of several chemical elements (H, D, He, C, N, O, Mg, Si, S, Ca, and Fe). The predictions of the models were compared with the $[\alpha/\text{Fe}]$ ratios and to the present day total and gas masses. Since there are very few available data concerning the metallicity distribution we compared our predictions to the MW disc distribution at the solar neighbourhood and to the metallicities of the observed stars. The observed stars were also used to infer if the predicted age-metallicity relations are reasonable, since there is also not enough data to derive this relation observationally.

The main conclusions can be summarized as follows:

- five of the six dSph galaxies are characterized by very low star formation efficiencies ($\nu = 0.005 - 0.5 \text{ Gyr}^{-1}$) with only Sagittarius having a higher one ($\nu = 1.0 - 5.0 \text{ Gyr}^{-1}$). In fact, Sagittarius is a unique galaxy when compared to the other dSphs of the sample. It is characterized by a much higher star formation efficiency. We predict for this galaxy a peak in the metallicity distribution well above (at $[\text{Fe}/\text{H}] \sim -0.8$ dex) the peaks in the other dSphs (at $[\text{Fe}/\text{H}] \sim -1.6 - -1.2$ dex). The AMR of this galaxy increases faster than the other dSphs with similar SF histories, reaching solar values shortly after 2 - 3 Gyr from the onset of the SF;

- a high wind efficiency, in the range $w_i = 6 - 15$, is required in order to reproduce the $[\alpha/\text{Fe}]$ ratios and the present day mass in the gas of the galaxies. The predicted $[\alpha/\text{Fe}]$ vs. $[\text{Fe}/\text{H}]$ plots show a rather short plateau at low metallicities until a sharp decrease occurs at higher metallicities. This sudden decrease in the abundance ratios is a consequence of the occurrence of intense galactic winds and

of the SNe Ia explosions. As soon as the wind starts, the SF decreases substantially and the rate of SNe II goes almost to zero halting the injection of α elements into the ISM, whereas SNe Ia continue producing and injecting iron peak elements into the ISM. These two facts cause the drop of the $[\alpha/\text{Fe}]$ ratio;

- the predicted age-metallicity relations imply that the stars of the dSphs reach solar metallicities on a time-scale of the order of 2 - 6 Gyr, depending on the particular SF history of the galaxy. The stars of the galaxies with SF starting at the same time of the formation of the galaxy (Sagittarius, Sextan, Sculptor and Ursa Minor) reach solar metallicities in a longer time-scale (typically 4 - 5 Gyr) and are characterized by a wider range of ages than the other two galaxies which have a SF starting at a galactic age of 6 Gyr. These two galaxies, Carina and Draco, produce stars with solar metallicities 2 to 3 Gyr after the beginning of the SF;

- the metallicity distribution of stars of dSphs exhibit a peak around $[\text{Fe}/\text{H}] \sim -1.8$ to -1.5 dex, with the exception of Sagittarius, which shows a peak around $[\text{Fe}/\text{H}] \sim -0.8$ dex. The typical peak is almost 1.5 dex below the one of the MW disc in the solar neighbourhood but similar to the value inferred for the halo of our Galaxy. The difference in the predicted peaks of the dSph galaxies and the MW disc is a consequence of the fact that the dSph galaxies are characterized by much lower SF efficiencies and to the occurrence of intense galactic winds which prevent the galaxies to form stars with metallicities higher than the one of the ISM of the galaxy shortly after the time at which the wind develops;

- the predicted metallicity distributions of stars exhibit a peak in the same range of metallicity of the observed stars, implying that the majority of stars are formed in the same range of the observed ones, if a Salpeter IMF is adopted. A Scalo-like IMF, as adopted in most models for the MW, predicts peaks at too low metallicities if compared with the available observations.

ACKNOWLEDGMENTS

We thank Antonio Pipino and Cristina Chiappini for reading the manuscript and for the comments on the paper. G.A.L. acknowledges financial support from the Brazilian agency FAPESP (proj. 00/10972-0). F.M. acknowledges financial support from INAF Project “Blu Compact Galaxies: primordial helium and chemical evolution” and from COFIN2003 from the Italian Ministry for Scientific Research (MIUR) project “Chemical Evolution of Galaxies: interpretation of abundances in galaxies and in high-redshift objects”.

REFERENCES

Bonifacio P., Hill V., Molaro P., Pasquini L., Di Marcantonio P., Santin P., 2000, *A&A*, 359, 663
 Bonifacio P., Sbordone L., Marconi G., Pasquini L., Hill V., 2004, *A&A*, 414, 503
 Carney B.W., Laird J.B., Latham D.W., Kurucz R.L., 1987, *AJ*, 94, 1066
 Chiappini C., Matteucci F., Gratton R. 1997, *ApJ*, 477, 765
 Cuisinier F., Maciel W.J., Kppen J., Acker A., Stenholm B., 2000, *A&A*, 353, 543
 Dolphin A.E., *MNRAS*, 2002, 332, 91

Edvardsson B., Andersen J., Gustafsson B., Lambert D.L., Nissen P.E., Tomkin J., 1993, *A&A*, 275, 101
 Greggio, L., Renzini, A., 1983, *A&A*, 118, 217
 Grevesse N., Sauval A.J., 1998, *Space Science Reviews*, 85, 161
 Hernandez X., Gilmore G., Valls-Gabaud D., 2000, *MNRAS*, 317, 831
 Kotoneva E., Flynn C., Chiappini C., Matteucci F., 2002, *MNRAS*, 336, 879
 Laird J.B., Rupen M.P., Carney B.W., Latham D.W., 1988, *AJ*, 96, 1908
 Lanfranchi G., Matteucci F., 2003, *MNRAS*, 345, 71
 Maciel, W.L., 1999, *A&A*, 351L, 49
 Mateo M.L., 1998, *ARA&A*, 36, 435
 Matteucci F., 1992, *ApJ*, 397, 32
 Matteucci F., 1996, *FCPh*, 17, 283
 Matteucci F., Tornambé A., 1987, *A&A*, 185, 51
 Matteucci F., Brocato E., 1990, *ApJ*, 365, 539
 Matteucci F., Romano D., Molaro P., 1999 *A&A*, 341, 458
 Nomoto K., Hashimoto M., Tsujimoto T., Thielemann F.-K., Kishimoto N., Kubo Y., Nakasato N., 1997, *Nucl. Phys. A*, 616, 79
 Pagel B.E.J., 1989, *RMxAA*, 18, 161
 Ratag M.A., Pottasch S.R., Dennefeld M., Menzies, J., 1997, *A&AS*, 126, 297
 Recchi S., Matteucci F., D’Ercole A., 2001, *MNRAS*, 322, 800
 Recchi S., Matteucci F., D’Ercole A., Tosi M., 2002, *A&A*, 384, 799
 Rocha-Pinto H.J., Maciel W.J., 1996, *MNRAS*, 279, 477
 Salpeter E.E., 1955, *ApJ*, 121, 161
 Scalo J.M., 1986, *FCPh*, 11, 1
 Schmidt M., 1963, *ApJ*, 137, 758
 Smecker-Hane T., Mc William A., 1999, in Hubeny I. et al., eds. *Spectrophotometric Dating of Stars and Galaxies*, ASP Conference Proceedings, Vol. 192, p.150
 Shetrone M., Côté P., Sargent W.L.W., 2001, *ApJ*, 548, 592
 Shetrone M., Venn K.A., Tolstoy E., Primas F., 2003, *AJ*, 125, 684
 Sommer-Larsen J., 1991, *MNRAS*, 249, 368
 Sommer-Larsen J., Yoshii Y., 1990, *MNRAS*, 243, 468
 Thielemann F.K., Nomoto K., Hashimoto M., 1996, *ApJ*, 460, 408
 Tinsley B.M., 1980, *FCPh*, 5, 287
 Tolstoy E., Venn K.A., Shetrone M., Primas F., Hill V., Kaufer A., Szeifert T., 2003, *AJ*, 125, 707
 Tosi M., 1988, *A&A*, 197, 33
 vand en Bergh S., 1962, *AJ*, 67, 486
 Van den Hoeck L.B., Groenewegen M.A.T., 1997, *A&AS*, 123, 305
 Wyse R.F.G., Gilmore G., 1995, *AJ*, 110, 2771

This paper has been produced using the Blackwell Scientific Publications L^AT_EX style file.